Precision Measurement of the Recoil Energy Spectrum from the Decay of He^6

C. H. JOHNSON, FRANCES PLEASONTON, AND T. A. CARLSON
Oak Ridge National Laboratory, Oak Ridge, Tennessee
(Received 28 June 1963)

The energy spectrum of recoil ions from the β^- decay of He^6 was observed repeatedly under a variety of operating conditions with a spectrometer which uses a tandem arrangement of magnetic and electrostatic analysis. Analyzed ions were detected with an electron multiplier. A composite spectrum is formed from the several observations, random errors are assigned on the basis of the observed fluctuations, and four parameters are adjusted to give the best fit of theory to experiment. These parameters are the maximum β^- energy W_0, an electron-neutrino correlation coefficient α, a normalization constant, and a detector parameter. The analysis gives $\alpha=-0.3343\pm0.0030$, where the uncertainty represents a careful evaluation of both random and systematic effects. The conclusion is reached, with "68% posterior probability," that the limit to the tensor interaction is $(|C_T|^2+|C_T'|^2)/(|C_A|^2+|C_A'|^2)\leq 0.4\%$. If one assumes that there is no tensor interaction but that higher order terms may be present, then one can conclude from a plane-wave $(Z=0)$ approximation for the He^6 decay that $b=-(0.5\pm1.3)(2M)^{-1}$, where b is a second-order term defined in Gell-Mann's paper on weak magnetism, and M is the ratio of nucleon-to-electron mass.

1. INTRODUCTION

A GENERALIZATION of Fermi's original theory of β decay allows for five different covariant interactions whose strengths are free parameters in the theory. These interactions are called scalar (S), vector (V), tensor (T), axial-vector (A), and pseudoscalar (P). Interactions S and V can be effective in the allowed Fermi transitions, and interactions T and A can enter into allowed Gamow-Teller transitions; there is no P interaction in allowed transitions. The most direct measurement of the relative strengths of the interactions is the observation of the angular correlation between the two leptons. In an allowed transition with the emission of β particles with velocity v, the correlation has the form $1+\alpha(v/c)\cos\theta$ where α is -1, $+1$, $+\frac{1}{3}$, and $-\frac{1}{3}$ for pure S, V, T, and A, respectively. In a measurement of α one infers the neutrino direction from observations of the recoil nucleus. Serious technical difficulties arise in the detection of the low-energy recoil ions; thus, although many early attempts were made to determine the relative strengths of the interactions, conclusive recoil measurements were not made until after the discovery[1] of nonconservation of parity.

The nonconservation of parity implies that the emitted leptons may be polarized. The first parity experiment[1] implied that the electrons have a negative polarization whose magnitude is about the maximum allowed by nonconservation of parity. Soon thereafter, the two-component neutrino theory[2-4] and the $V\pm A$ theories[5-7] were proposed. These elegant theories suggest that the polarization of the $\beta^\pm$ particles are exactly $\pm v/c$ and that the polarizations of the massless neutrinos are exactly $+100\%$ or -100%. In the $V\pm A$ theories the neutrino polarization is opposite in sign to that of the accompanying β particle.

Experimental confirmation of the predicted electron polarization has come from a variety of experiments with ever increasing precision.[8] Recent very careful measurements by Brosi *et al.*[9] give a polarization of $(-0.990\pm0.009)v/c$ for the β^- particles from P^{32}. Experimental determination of the neutrino polarization also came quickly but with somewhat less precision than for the electron. In this regard the electron-neutrino correlation now has a significance in addition to its usual role of assigning the interaction strengths. The coefficients $(-\alpha)v/c$ for Fermi and $(3\alpha)v/c$ for Gamow-Teller transitions are the average relative helicities of the leptons; thus, given the polarization $\pm v/c$ for the $\beta^\pm$ particles, the coefficients $\mp\alpha$ or $\pm3\alpha$ become the neutrino polarizations in the allowed Fermi and Gamow-Teller transitions, respectively. A measurement of the electron-neutrino angular correlation can be interpreted in terms of the neutrino polarization.

Within a year or two after the new theories were advanced, it was clear experimentally[8] that the interactions are essentially V and A; thus, within the experimental uncertainties, the neutrinos are 100% polarized with sign opposite to that of the accompanying β particles. Allen *et al.*[10] found the $\beta-\nu$ correlation coefficients by observing the energy spectra of recoil ions from the decay of He^6, Ne^{19}, Ne^{23}, and Ar^{35}. The results supported the $V\pm A$ theory and limited the possible admixture of S and T intensities to about 10%. Goldhaber *et al.*[11] found from the observation of circularly polarized γ rays from the decay of Eu^{152} that the

[1] C. S. Wu, E. Ambler, R. W. Hayward, D. D. Hoppes, and R. P. Hudson, Phys. Rev. **105**, 1413 (1957).
[2] T. D. Lee and C. N. Yang, Phys. Rev. **105**, 1671 (1957).
[3] L. Landau, Nucl. Phys. **3**, 127 (1957).
[4] A Salam, Nuovo Cimento **5**, 299 (1957).
[5] R. P. Feynman and M. Gell-Mann, Phys. Rev. **109**, 193 (1958).
[6] E. C. G. Sudarshan and R. E. Marshak, Phys. Rev. **109**, 1860 (1958).
[7] J. J. Sakurai, Nuovo Cimento **7**, 649 (1958).
[8] O. Kofoed-Hansen and C. J. Christensen, in *Handbuch der Physik*, edited by S. Flügge (Springer-Verlag, Berlin, 1962), Vol. 41, Sec. 2.
[9] A. R. Brosi, A. I. Galonsky, B. H. Ketelle, and H. B. Willard, Nucl. Phys. **33**, 353 (1962).
[10] J. S. Allen, R. L. Burman, W. B. Herrmannsfeldt, P. Stähelin, and T. H. Braid, Phys. Rev. **116**, 134 (1959).
[11] M. Goldhaber, L. Grodzins, and A. W. Sunyar, Phys. Rev. **109**, 1015 (1958).

neutrinos accompanying K capture are negatively polarized; Markland and Page[12] confirmed these results. These measurements on Eu^{152} are particularly significant because they give the sign of the neutrino polarization without prior knowledge of the positron's polarization. Measurements[13,14] on Li^8 indicate that the T/A intensity ratio is less than 0.1. Our preliminary measurements[15] on He^6 showed the dominance of the A interaction. Ridley's early work[16] gave evidence for the T interaction in the decay of Ne^{23}; however, his later study[17] on He^6 revealed a systematic error in his Ne^{23} report and showed, with 90% confidence, that the T/A intensity ratio is less than 0.08. Experiments[18,19] on the directional asymmetries from the decay of polarized neutrons showed that the V and A terms are dominant and that the ratio of the Gamow-Teller to the Fermi coupling constants is -1.25 ± 0.05.

None of these measurements, which are related to the neutrino's polarization, have precision comparable to those on the electron polarization. This is not surprising; recoil or neutrino experiments are difficult because the recoil ion energy is very low, only a few hundred eV. As a result, most measurements are made with rare gases in order to avoid solid state or molecular effects on the recoil ions. A problem then arises as to the containment of the gaseous source which, because of the low ion energy, must be in vacuum communication with the detector. Various procedures may be used but the result is often the same, i.e., the intensity is too low or the signal-to-noise ratio is too low for a precision experiment. It was apparent, however, at the time of our preliminary report[15] that our apparatus was not restricted by lack of intensity or by an unfavorable signal-to-noise ratio. The Oak Ridge Research Reactor, which had just become available, provided a prolific source of He^6; and the apparatus, which was designed and used previously by Snell and Pleasonton,[20] was able to reduce the background to a fraction of the signal. Thus, we set out to make a recoil measurement with a precision comparable to that of the electron polarization measurements. Several obstacles had to be overcome in order to achieve this goal. The most serious obstacle has been related to the ion detector's efficiency, and this also is not surprising; the detection of low-energy ions has well-known difficulties.

The measurements reported here give the energy spectrum of recoil ions from the β^- decay of He^6, a nucleus which undergoes a pure allowed Gamow-Teller transition to a single final state. As reviewed in the next section, the theoretical recoil energy distribution is a function of the angular correlation coefficient α which, in turn, is related to the relative strengths of the T and A coupling constants. The result of our investigation has revealed no hint of the tensor interaction or any other effects not included in the presently accepted theory of allowed Gamow-Teller transitions.

Several related measurements were made concurrently with this work. The He^6 decay energy was found to be 3509 ± 4 keV and was reported elsewhere.[21] A related measurement[22] has given 0.797 ± 0.003 sec for the He^6 half-life. The charge spectrum for the recoil Li^6 ions was observed and was interpreted[23] in terms of the sudden change of nuclear charge and velocity. Finally, after the He^6 measurement was completed, one of us[24] measured the recoil-energy spectrum from the decay of Ne^{23}.

2. THEORY

Our procedure involves a least-squares analysis of the observed energy spectrum corrected for several small experimental effects. Perhaps the theory, which is required before the analysis begins, should contain all conceivable higher order terms which might be as large as the experimental uncertainties; however, such an all inclusive theory has not been published. Formulas including higher order terms have been derived[25,26] on the basis of the presently accepted conserved vector current theory but not for a general theory including both T and A interactions. Perhaps this is just as well; our conclusions might be quite vague if we introduced every conceivable effect, each with an adjustable parameter. Some assumptions are required; and our procedure is to use the usual theory of β^- decay including both T and A interactions in order to draw a conclusion on the relative strengths of the T and A coupling constants. Later, in the conclusion, we assume that there is no T interaction and draw some conclusions regarding the higher order terms in the conserved vector current theory.

In the general theory, the probability for emission of an electron with momentum $\mathbf{p}$ at an angle θ relative to the momentum $\mathbf{q}$ of the neutrino is

$$P(\mathbf{p},\mathbf{q})dWd\Omega = D_0F(Z,W)L_0(Z,W)pWq^2 \times\left(1+\frac{\beta}{W}+\alpha\frac{p}{W}\cos\theta\right)dWd\Omega, \quad (1)$$

where the units are, as usual, for zero neutrino mass,

[12] I. Marklund and L. A. Page, Nucl. Phys. **9**, 88 (1958/59).
[13] K. H. Lauterjung, B. Schimmer, and H. Maier-Leibnitz, Z. Physik **150**, 657 (1958).
[14] C. A. Barnes, W. A. Fowler, H. B. Greenstein, C. C. Lauritsen, and M. E. Nordberg, Phys. Rev. Letters **1**, 328 (1958).
[15] F. Pleasonton, C. H. Johnson, and A. H. Snell, Bull. Am. Phys. Soc. **4**, 78 (1959).
[16] B. W. Ridley, Nucl. Phys. **6**, 34 (1958).
[17] B. W. Ridley, Nucl. Phys. **25**, 483 (1961).
[18] M. T. Burgy, V. E. Krohn, T. B. Novey, G. R. Ringo, and V. L. Telegdi, Phys. Rev. **120**, 1829 (1960).
[19] M. A. Clark and J. M. Robson, Can. J. Phys. **38**, 693 (1960), and **39**, 13 (1961).
[20] A. H. Snell and F. Pleasonton, Phys. Rev. **100**, 1396 (1955).
[21] C. H. Johnson, F. Pleasonton, and T. A. Carlson, Nucl. Phys. **41**, 167 (1963).
[22] J. K. Bienlein and Frances Pleasonton, Nucl. Phys. **37**, 529 (1962).
[23] T. A. Carlson, F. Pleasonton, and C. H. Johnson, Phys. Rev. **129**, 2220 (1963).
[24] T. A. Carlson, Phys. Rev. (to be published).
[25] M. Gell-Mann, Phys. Rev. **111**, 362 (1958); **112**, 2139E (1958).
[26] Masato Morita, Nucl. Phys. **14**, 106 (1959).

$\hbar=m=c=1$. Here W is the total relativistic electron energy, $F(Z,W)$ is the Fermi Coulomb function, D_0 is a proportionality constant, β is the coefficient of Fierz interference, and α is the angular correlation coefficient. The term $L_0(Z,W)$ is rather standard notation[26] for a factor which is nearly unity but has a very small energy dependence for a nucleus of finite size and charge.

A transformation to variables which are appropriate for our recoil experiment is made by use of the equations for energy and momentum conservation:

$$Q^2=p^2+q^2+2pq\cos\theta \tag{2}$$

and

$$W+E_r+q=W_0+E_r(\max), \tag{3}$$

where W_0 is the maximum β^- energy, and E_r and Q are the energy and momentum of the recoil ion. The recoil-energy distribution is then found by integrating over W, keeping E_r fixed with the very good approximation that $E_r(\max)=E_r$ in Eq. (3). The integration is readily performed[27,28,10] for $F(Z,W)=L_0(Z,W)=1$, and small energy-dependent correction terms related to $F(Z,W)$ and $L_0(Z,W)$ are estimated with the assumption that the Gamow-Teller interaction is pure axial vector, i.e., $\alpha=-\frac{1}{3}$. Integration yields the recoil-energy distribution

$$\begin{aligned}P(E_r)dE_r&=D_1F(E_r)[N_1(E_r)+\alpha N_2(E_r)+\beta N_3(E_r)]dE_r\\&=D_1F(E_r)N(E_r,W_0,\alpha,\beta)dE_r,\end{aligned} \tag{4}$$

where $N_1(E_r)$, $N_2(E_r)$, and $N_3(E_r)$ are given in Appendix A. Rose's[29] tabulation for the Fermi function was used to derive the term $F(E_r)$ which is shown in Fig. 1. Terms arising from the energy dependence of $L_0(Z,W)$ are omitted because their variation is negligible. In the least-squares analysis the Fierz term β is also assumed to be negligible; however, an uncertainty is assigned to α which includes the effect of the experimental uncertainty[30] in β.

The value of α from the least-squares analysis is then used to estimate the relative T and A contributions in the expression[31]

$$\begin{aligned}3\xi\alpha=&|C_T|^2+|C_T'|^2-|C_A|^2-|C_A'|^2\\&\pm\frac{2e^2Zm}{\hbar cp}\,\mathrm{Im}(C_TC_A^*+C_T'C_A'^*),\end{aligned} \tag{5}$$

where

$$\xi=|C_T|^2+|C_T'|^2+|C_A|^2+|C_A'|^2. \tag{6}$$

The C's are the usual coupling strengths. The last term in Eq. (5) is neglected because it contains the fine structure constant and because the essential validity of time reversal invariance[18] requires the imaginary components to be small.

[27] O. Kofoed-Hansen, Phys. Rev. **74**, 1785 (1948).
[28] M. E. Rose, ORNL-1593, 1953 (unpublished).
[29] M. E. Rose, in *Beta- and Gamma-Ray Spectroscopy*, edited by K. Siegbahn (Interscience Publishers Inc., New York, 1955), pp. 271–291.
[30] M. K. Ramaswamy, Indian J. Phys. **33**, 285 (1959).
[31] J. D. Jackson, S. B. Treiman, and H. W. Wyld, Jr., Nucl. Phys. **4**, 206 (1957).

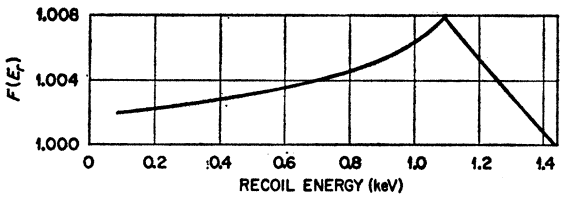

FIG. 1. Recoil energy dependence resulting from the Fermi Coulomb function $F(Z,W)$. The function $F(E_r)$, which appears in the theoretical energy spectrum in Eq. (4), was calculated by use of Rose's tables (Ref. 28) for $Z=3$ and normalized to unity at the end point.

3. EXPERIMENTAL

A. Apparatus

The He^6 is produced in the $Be^9(n,\alpha)He^6$ reaction by irradiating about 150 g of very fine BeO powder in the Oak Ridge Research Reactor. A continuous stream of water vapor sweeps the He^6 to the laboratory where a series of three cold traps containing ice, dry-ice, and a mixture of liquid and solid N_2 removes the water and most of the radioactive contaminants. In addition, most of the decomposed H_2O is removed by passing the gas over hot Cu and CuO. The He^6 generator and gas-handling system, which are fully described elsewhere,[32] are shown schematically in Fig. 2 together with a diagram of the recoil spectrometer which is essentially the same as that described previously by Snell and Pleasonton[20] and by Carlson *et al.*[23]

An extremely stable supply of the source gas is delivered continuously to the large source volume. A small fraction of the Li^6 ions, recoiling from the decay of the He^6 gas, emerges through a $\frac{1}{2}$-in. hole near the tip of the cone forming a beam which is analyzed by a tandem

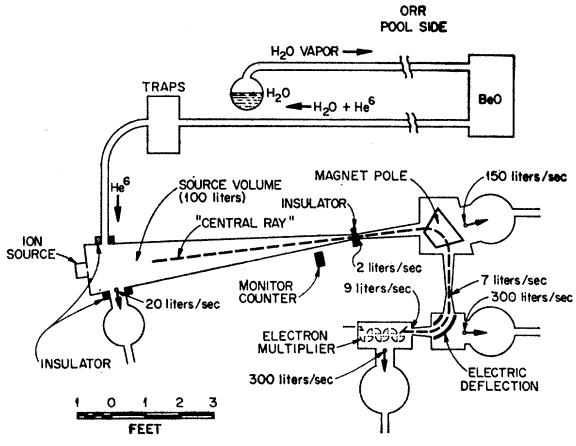

FIG. 2. Experimental apparatus. The He^6 produced in a reactor by the $Be^9(n,\alpha)He^6$ reaction is carried by a continuous stream of water vapor to the laboratory where the vapor is removed and the He^6 is left to decay in the conical source volume. A proportional counter monitors the source activity. Recoil Li^6 ions undergo magnetic and electrostatic analysis and are detected by a secondary electron multiplier. Three stages of differential pumping reduce the background of atoms which decay near the detector.

[32] Frances Pleasonton and C. H. Johnson (to be published).

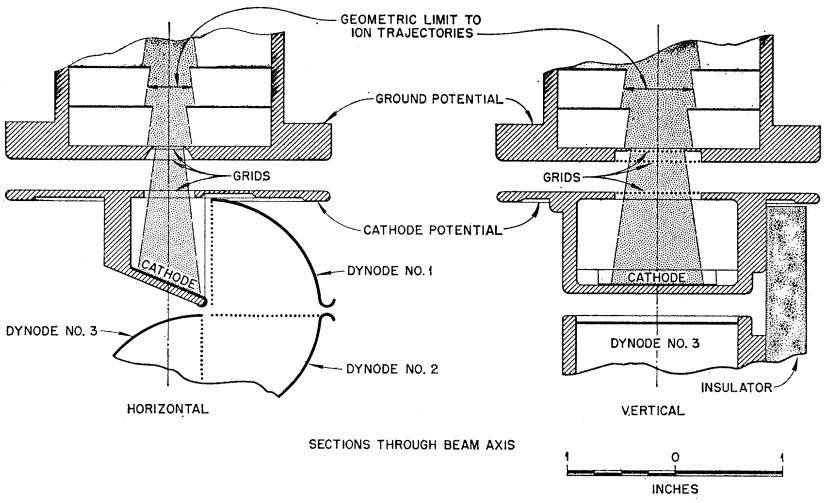

FIG. 3. Horizontal and vertical sections of the entrance and cathode geometry for the box-and-grid electron multiplier. The analyzed ions enter through a 0.23-in. by 0.45-in. aperture and are accelerated to several keV by the cathode-to-ground potential between grids of horizontal wires lying in the two potential planes. The "2-grid" counter had only these two grids whereas the "3-grid" counter has the additional one shown between the aperture and ground plane.

arrangement of stigmatic-focusing magnetic and electrostatic deflectors. The ions are then accelerated and then detected by a secondary-electron multiplier whose counts are normalized to those of a proportional counter near the source volume. This double analysis is valuable because it not only discriminates against recoils from possible radioactive contaminants but also distinguishes the various charge species of the Li^6 recoils themselves.

Strong differential pumping results in a gratifyingly low background from gas diffusing to the vicinity of the detector. Continuous pumping on the source volume maintains a vacuum of about 10^{-6} Torr and helps to remove any H_2O dissociation products or longer lived activities, such as N^{16}, that may not be completely eliminated in the gas purification system. An electrically field-free state in the source volume is assured by shielding it from all insulating materials and by using only Hg diffusion pumps. Although shielding against stray magnetic fields is provided for the spectrometer, it is, unfortunately, omitted for about two-thirds of the source volume; this oversight introduces a small uncertainty in the measurements (Sec. 4 I).

Thin baffles are placed along the interior walls of the source and of the spectrometer to prevent reflection of the ions into the beam from the walls of the vacuum chambers. They are omitted, however, in the electrostatic analyzer because the beam misses the deflector plates when their field is set properly. The exit aperture of the source volume is only 0.002 in. thick in order to minimize reflections at the object plane of the magnet, and the 0.23-in. by 0.45-in. image aperture at the detector is made with a knife edge to minimize reflections into the detector.

Stabilized supplies furnish all the voltages required for the accelerating and deflecting fields, and also for operation of the multiplier. The potentials of the source volume and of the deflector plates are measured by means of precision resistance dividers, a type-K potentiometer, and a standard cell. The precision of these measurements varies from 0.01 to 0.04% except for observations on nonaccelerated ions of less than 0.2-keV energy, where it rises to 0.06%. A well-regulated supply furnishes the current for the magnet coils, and measurements of the field strengths are made by a proton nuclear resonance fluxmeter whose frequencies are measured to ± 1 kc/sec. Observations of the singly charged Li^6 ions required field strengths corresponding to resonant frequencies of about 0.89 to 4.68 Mc/sec.

Almost negligible losses or gains of the Li^+ ion beam occur from charge transfer and scattering in the source volume and in the analyzers. At normal operating pressures of 1.2×10^{-6} Torr in the source volume and 7×10^{-7} Torr in the analyzers, there are about 10^{13} molecules/cm^2 along the beam's path from the center of the cone to the detector. The cross section for losses by charge transfer[33] is about 10^{-18} cm^2/molecule for Li^+ and about[34] 6×10^{-16} for Li^{++}; the latter leads to negligible enhancement of the Li^+ beam because of the low Li^{++}/Li^+ intensity ratio, 1/10. Inelastic collisions without charge transfer are indistinguishable from elastic scattering. Because elastic scattering is predominantly forward,[35] the effective cross section for scattering out of the analyzer's acceptance angle is less than the total elastic cross section, which is about 30×10^{-16} cm^2/molecule. Losses of ions scattering away from the apertures at the exit of the source volume and at the detector entrance are largely compensated by in-scattering. Such compensation does not occur at the magnet's image plane where the aperture closely matches the beam size. A small correction for scattering in the residual gas in the analyzers is given in Sec. 4 D.

The detector is an electron multiplier with a Ag-Mg cathode followed by ten stages of electron multiplication

[33] Klaus Bethge, Z. Phys. **162**, 34 (1961).
[34] S. K. Allison, J. Cuevas, and M. Garcia-Munoz, Phys. Rev. **120**, 1266 (1960).
[35] H. S. W. Massey and E. H. S. Burhop, *Electronic and Ionic Impact Phenomena*, (Clarendon Press, Oxford, England, 1952).

in a box-and-grid array. Two stabilized voltage supplies are required. One of these is isolated from ground and furnishes the multiplier voltage, and the other, which can be cascaded with the first, provides a field for accelerating the ions to several keV before they strike the cathode. A mu-metal cylinder shields the multiplier from stray magnetic fields and various conductors shield against static charges on insulators. Signals from the anode are fed to a pulse amplifier which uses double-delay line differentiation. Measurements by the two-source method gave a dead-time of 2.7 ± 0.6 μsec for the amplifier and scaler. A rubber dam was used in the design of the multiplier's entrance and cathode geometry which is shown in vertical and horizontal cross section in Fig. 3. Geometric limits for the analyzed ion trajectories are indicated. The acceleration of the ions occurs between parallel plates whose ratio of diameter to separation is 10 to 1. Grids of 0.001-in. wires on 0.031-in. centers are mounted in the planes of the plates so that the field is nearly normal to the plates. The wires are mounted horizontally so that the local fields at the wires cause only vertical deflections; the cathode's vertical dimension is oversize in order to intercept these deflected ions. The beam-defining aperture, which is also the image aperture for the electrostatic analyzer, is in essentially field-free space 0.1 in. from the ground plane.

The cathode geometry was designed with the objective that all ions accelerated through the grids strike the cathode and that all secondary electrons, except those hitting the dynode grid, be collected to the first dynode. Care was taken in the preparation of the cathode so that the surface appeared uniform; and, after installation in the spectrometer, the electron collection efficiency was studied by observing the counting rate as a function of the cathode-to-dynode voltage. The counting rate reached a plateau starting at 250 V, and subsequent operation was in the plateau region. As an added precaution against failure to detect secondary electrons, the over-all gain of the multiplier and its amplifier was increased until the counting rates were essentially independent of the amplifier's discriminator level. Figure 4 shows typical integral bias curves observed with singly charged Li^6 ions of 3.3- and 6.1-keV energy. Points are shown for data obtained with two

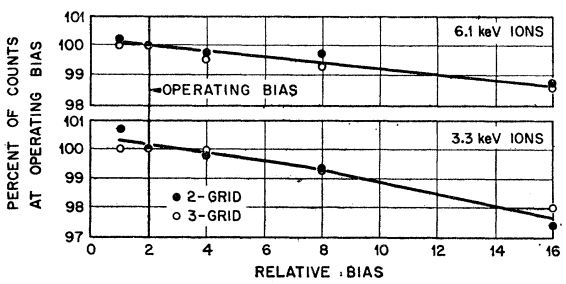

FIG. 4. Integral bias curves measured at two energies of Li^6 ions and for both grid structures of the multiplier. The data are corrected only for background.

different grid geometries, and the agreement of the two sets of data indicates that the cathode sensitivity was not altered during the changing of the grids.

As will be seen in Sec. 4 E, our knowledge of the detector's efficiency is of paramount importance in the analysis. Unfortunately, acceleration of the ions at the detector's entrance, which is essential for efficient secondary electron emission, inevitably introduces focusing and transmission effects which alter the beam configuration; for a given incident beam, the effect is a function of the energy multiplication imposed by the grid field. It was hoped that the detector's efficiency would be independent of focusing effects; however, measurements which are described in Sec. 4 F showed a focus dependence. These measurements were made with a "2-grid" counter which had grids only in the planes of the two plates. The third grid, which is shown between the aperture and ground plane, was then installed, and the detector was found to have very little focus dependence. The data analyzed in this paper were taken with both the "2-grid" and the "3-grid" counters. Field plots, which were made with an electrolytic-tray model after the experiment was completed, indicate that the third grid was not important but, rather, that the newly wound ground-plane grid wires probably replaced ones that were sagging out of line.

B. Measurements

The source activity was adequate for many repeated measurements of the spectrum and for a detailed investigation of the equipment. In particular, detailed detector efficiency curves were obtained and are discussed in Sec. 4 E. In order to minimize slow drifts in signal-to-background ratios, all data were taken by alternating short intervals of background and signal-plus-background observations. Backgrounds were normally measured with a negative bias of 1.6 kV applied to the source in order to remove the source ions from observation without disturbing other operating conditions. Each counting interval was about 1 or 2 min and was controlled by the accumulation of a predetermined number of monitor counts, about 1 or 2 times 10^5. Backgrounds were then subtracted to give the net signal for the series of intervals and the data were normalized to the number of monitor counts. A very small correction is made for dead-time losses in the detector. Dead-time corrections are not required for the monitor because its counting rate is nearly constant during each set of measurements; however, a small correction is required for a linear dependence of monitor rate on source potential. This anomalous monitor effect could result from a true change in source activity or a false change in monitor efficiency; but, since neither explanation seems reasonable, a correction is applied which lies midway between the limiting explanations. (Section 4 I gives the uncertainties corresponding to these limits.) If the correction was not made, the coefficient α would differ by

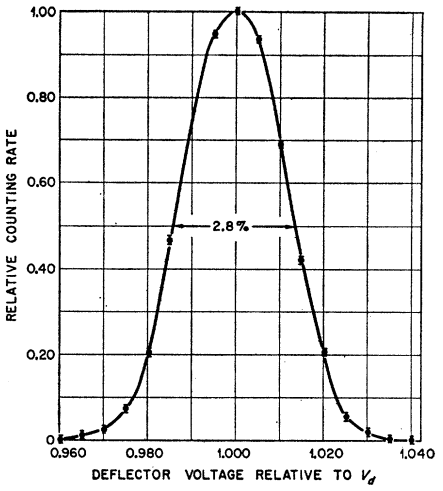

FIG. 5. Analyzer transmission curve for nonaccelerated recoil ions, observed at a fixed magnet setting corresponding to ion energies of about 1.2 keV. The counting rate is plotted versus the ratio of the applied deflector voltage to the one required for maximum transmission of the beam.

0.2% from our final value. This procedure gives a raw data point; further energy-dependent corrections are given in Sec. 4 for the points that determine the recoil energy spectrum.

The matching constant required for mutual alignment of the two analyzers is found by setting the magnet to accept ions from the continuous recoil spectrum and then tuning the electrostatic analyzer for maximum transmission. Figure 5 illustrates a typical transmission peak for the Li^+ ions at 1.2-keV recoil energy. The net signal is plotted versus the relative electrostatic deflector voltage for a fixed magnet setting. Peaks obtained for ions that were accelerated to twice their recoil energy before analysis are slightly narrower than this peak because of a decrease of beam divergence. Tracking of the analyzers at other energies is then accomplished by varying the deflector plate potentials with the square of the resonance frequency. Care must be exercised because the proton resonance probe sees only a sample magnetic field rather than the correct average, but careful investigations showed that good tracking is obtained by operating the magnet on a given hysteresis loop. New transmission curves were obtained whenever an unusual current adjustment moved the operation to a new loop. For this reason the electrostatic rather than the magnetic analyzer is the basic or stable element of the analyzer. Measurements at low magnetic fields use a second resonance probe which is in a slightly different position in the magnetic field and requires a slightly different matching constant.

With the available activity the recoil spectrum could be scanned with good statistics in a few hours; hence, we were able to make repeated measurements with some variation of the experimental parameters. One variation has already been indicated: the use of both a 2-grid and a 3-grid counter. Another important variation was to preaccelerate the ions to about twice their recoil energy before analysis. Of course, preacceleration introduces a focus effect, but this does not distort the spectrum if the source potential is varied directly with the energy of the ions being analyzed. Preacceleration alters the energy and divergence of the ion beam in the analyzer chamber, improves the signal-to-background ratio, and alters the position of the end point; thus, in many ways, it provides an independent measurement of the spectrum.

Measurements were usually made at 16 recoil energies from 0.1 to 1.3 keV. Possible systematic effects of slow drifts in the equipment were minimized by taking data points in somewhat random order. About 100 spectra were observed; however, only the last 26 of them are accompanied by detector-efficiency curves that are complete enough to permit analysis. These 26 spectra have been reduced to 12 sets of data corresponding to the 12 modes of operation that were used. These modes are summarized in Table I. The sets are grouped according to the degree of preacceleration; and the columns give the set number, the grid structure of the detector, the number of energy points, the degree of energy multipli-

TABLE I. Modes of spectrometer operation used in observing the energy spectrum of Li^+ recoil ions.

Set no.	Multiplier grid structure	Number of energies observed	Range of detector parameters: Energy multiplication ratio at the grids: y	Range of detector parameters: Ion energy at the cathode: E_c (keV)
		Nonaccelerated		
1	2-grid	16	6.8–31.0	3.1– 8.9
2	2-grid	16	1.7–22.0	2.2
3	2-grid	14	6.0–34.2	4.8– 7.8
4	2-grid	16	3.7–36.0	3.6– 4.8
5	3-grid	16	1.7–22.0	2.2
		Preaccelerated		
6	2-grid	15	3.9–17.5	4.9–10.2
7	2-grid	10	2.3–11.4	3.2– 6.1
8	2-grid	16	1.7–22.0	4.4
9a	2-grid	12	3.9–17.5	4.7– 8.9
9b	2-grid	10	2.3–11.4	3.2– 6.5
9c	2-grid	5	1.7–15.6	4.4
10	3-grid	16	1.7–22.0	4.4
11	3-grid	10	3.9–11.4	4.7–10.2
12	3-grid	11	2.3–11.4	3.3– 6.1

TABLE II. Typical ranges of data in the counting rate of the ion detector.

Type of ions	Recoil energy (keV)	Counting rates (counts/sec): Signal plus background	Counting rates (counts/sec): Background	Ratio of signal-to-background
Nonaccelerated	0.1	145	124	0.2
	1.2	518	132	2.9
Preaccelerated	0.1	220	145	0.5
	1.2	1610	130	11.3

cation at the detector grids, and the energies of the ions when they were detected. Set No. 9 is unusual in that the source volume was shortened to about one-third of its normal length. Typical extremes of the multiplier's counting rate and its signal-to-background ratio are given in Table II for both nonaccelerated and preaccelerated ions of 0.1 and 1.2-keV recoil energy. The corresponding monitor rates were about 2100 counts/sec.

Figure 6 shows the spectrum of singly charged Li^6 recoil ions as a function of the average recoil energy of the analyzed ions; the data correspond to set No. 10 in Table I. Data shown by open circles near the end point are not part of the set but were obtained on another day for the purpose of the end-point analysis. Uncertainties for counting statistics are smaller than the dimensions of the points. Corrections have not been made for the energy-dependent effects which are discussed in the next section, but these corrections would not be discernible on this linear plot. The curve is the theoretical spectrum, $B\bar{E}_r N(\bar{E}_r, W_0, \alpha)$, which is plotted by choosing the normalization constant B and the maximum β energy W_0 to fit the data. The constant α is chosen to be $-\frac{1}{3}$, corresponding to the axial-vector interaction, and the Fierz term β is assumed to be zero. Clearly the data agree well with the theory.

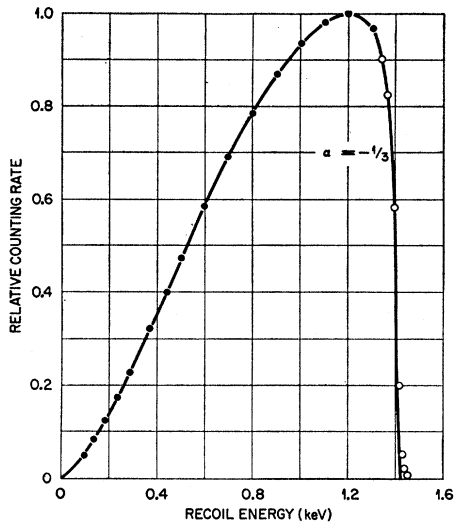

FIG. 6. Spectrum of singly charged Li^6 ions as a function of the average recoil energy of the ions transmitted by the analyzers. Ions were accelerated to about twice their recoil energy before analysis. Data indicated by solid dots are from four observations of the spectrum which form set No. 10 of data in Table I. Data indicated by open circles near the end point were obtained separately. The only significant correction that has been made is for background; other corrections in the analysis are not discernible on a linear plot. Uncertainties from counting statistics are less than the point sizes. The theoretical curve is plotted for $\alpha=-\frac{1}{3}$ with the normalization constant and the end-point W_0 chosen to give a good fit of theory to experiment.

4. ANALYSIS

In the foregoing section the method of observing each data point was described and corrections were made for background, dead-time losses, and an anomalous monitor effect. Now we are concerned with a least-squares analysis of these data following further corrections which are related to the spectrum, i.e., to the relationship among the data points. Section A introduces a general expression for the analysis. Small corrections for the energy dependence of the charge spectrum, effects of finite energy resolution, and scattering in the residual gas are given in Secs. B, C, and D; Sec. C also contains the end-point analysis for W_0. Sections E and F include important corrections for detector efficiencies and introduce an adjustable detector parameter. Section G presents the least-squares analysis, and Sec. H examines the results for internal consistency. Finally, in Sec. I, an uncertainty is assigned for the correlation coefficient α.

A. General Formulation

We will begin with a general integral which is written under the assumption that the ions are not deflected by spurious fields, nor are they scattered by residual gas in the source or from the wall baffles into the detector. Effects of scattering from gases in the analyzer chamber will be included. (Later an uncertainty will be allowed for the effects of the earth's magnetic field.) The only other forces on the ions are those resulting from four legitimate fields, namely, the preaccelerating field caused by the source potential V_s, the magnetic deflecting field H of the analyzer, the electrostatic deflecting field determined by the voltage V_d, and the field produced by the detector grid voltage V_g. For simplicity let us choose energy units such that the electron charge is unity; then singly charged ions which recoil through the source aperture with energy E_r are preaccelerated to an energy $E_a=E_r+V_s$ for the analysis and to a final energy $E_c=E_a+V_g$ for detection at the cathode.

The probable counting rate for the detection of singly charged recoil ions which originate in the source is

$$u(V_s,V_d,V_g)=B_1\int P(E_r)A_1(E_r)S(E_a)t\left(\frac{E_a}{E_r},\frac{E_a}{V_d}\right)\times m\left(\frac{E_a}{E_r},\frac{E_a}{V_d},\frac{E_a}{E_c},E_c\right)dE_r, \quad (7)$$

where $B_1P(E_r)dE_r$ is the probable rate at which recoil ions of energy E_r to E_r+dE_r leave the source aperture, and $A_1(E_r)$ is the singly charged fraction of these ions. The factor $t(E_a/E_r,E_a/V_d)$ for transmission of the ions through the analyzer chambers at zero pressure to the detector aperture is also a function of E_a/H^2; but since $V_d\propto H^2$ for the matched analyzers, only the two ratios are indicated. The fraction, $1-S(E_a)$, of the transmitted ions is scattered out by the residual gas. The efficiency function m for transmission through the detector grids and detection at the cathode depends primarily on the grid variable E_a/E_c and on the final

energy E_c at the cathode; however, the variables E_a/E_r and E_a/V_d are also included in order to indicate a possible dependence on the incident ion trajectories. Variations of the efficiency with the multiplier and amplifier gains and with the discriminator bias level are not shown because these were constants during the experiment.

The most rapidly varying function in the integrand is t which is finite for only a limited range of the analyzer variable E_a/V_d. The recoil-energy distribution $P(E_r)$ is essentially linear in this limited range, except near the end point of the distribution, and the other terms in the integrand are nearly constant; thus, except near the end point, the product of all terms other than the transmission factor can be approximated by a linear function. Integration yields

$$u(V_s,V_d,V_g)=B_1\bar{E}_a v\left(\frac{\bar{E}_a}{\bar{E}_r}\right)R\left(\frac{\bar{E}_a}{\bar{E}_r},\bar{E}_r\right)P(\bar{E}_r)A_1(\bar{E}_r)\times S(\bar{E}_a)m\left(\frac{\bar{E}_a}{\bar{E}_r},\frac{\bar{E}_a}{V_d},\frac{\bar{E}_a}{\bar{E}_c},\bar{E}_c\right), \quad (8)$$

where the energies are now averages. $\bar{E}_a$ is the average energy of ions transmitted through the analyzer, and $\bar{E}_r$ and $\bar{E}_c$ are the corresponding average recoil and final energies. The average $\bar{E}_a$ is $[K(V_s/V_d)]^2V_d$, where the analyzer's calibration coefficient K[2] actually has little, if any, dependence on V_s/V_d. A transformation of variables allows the equation to be written in the simpler form

$$U(\bar{E}_r,x,y)=B_1\bar{E}_r V(x)R(x,\bar{E}_r)P(\bar{E}_r)\times A_1(\bar{E}_r)S(x\bar{E}_r)M(x,y,\bar{E}_c), \quad (9)$$

where x and y are energy multiplication factors; x is the ratio $\bar{E}_a/\bar{E}_r$ imposed by the preacceleration voltage V_s, and y is the ratio $\bar{E}_c/\bar{E}_a$ imposed by the grid voltage V_g. A resolution factor $R(x,\bar{E}_r)$ has been inserted into Eq. (9) to permit a later correction near the end point where the linear approximation is not valid; for most recoil energies this factor is unity.

Substitution of the theoretical energy spectrum from Eq. (4), assuming the Fierz term β is zero, gives

$$B_2(x)\bar{E}_r N(\bar{E}_r,W_0,\alpha)=\frac{U(\bar{E}_r,x,y)}{F(\bar{E}_r)A_1(\bar{E}_r)R(x,\bar{E}_r)S(x\bar{E}_r)M(x,y,\bar{E}_c)}, \quad (10)$$

which is the basic equation for the analysis. For a given x, the term on the left is a theoretical expression in the variable $\bar{E}_r$. The factor $B_2(x)$ is a constant of proportionality for any given spectrum: $x=1$ for nonaccelerated ions and $x\approx 2$ for accelerated ions. The term on the right is essentially the observed spectrum. (Of course, the equality holds only in the limit of an infinite number of observations.) The numerator is the observed counting rate corrected for background, dead time losses, and the anomalous monitor effect and normalized to the monitor counts. The term $F(\bar{E}_r)$, which results from the Fermi function, has been transposed to the right-hand or experimental side of the equation in order that the left-hand side retain a simple analytic form. The remaining four corrections in the denominator will be discussed in the following five sections.

B. Correction for the Charge Spectrum

A separate paper[23] gives the relative abundances of singly, doubly, and triply charged ions which were observed with this apparatus concurrently with the present measurements. The analysis, which is related to the phenomenon of electron shakeoff following β^- decay, gave

$$A_1(\bar{E}_r)=(0.899\pm0.002)-(4.5\pm0.7)10^{-6}\bar{E}_r, \quad (11)$$

where $\bar{E}_r$ is in eV. If this energy dependence were neglected in the analysis, our final α would be about 0.6% more negative.

C. End-Point Analysis for W_0 and for the Resolution Correction

The spectrum varies slowly over the width of the analyzer's transmission function except in the region above about 1.3 keV where it descends abruptly to the end point. Since a linear approximation is not valid in this region, a separate analysis is made by folding the theory into the transmission or resolution function in the integral of Eq. (7). The procedure, which gives a maximum β^- energy of 3508±4 keV, has already been reported,[21] and only a few additional comments are required. The analysis was made for $\alpha=-\frac{1}{3}$; in principle, an iterative procedure should now be followed until the entire spectrum uses a self-consistent α, but this is unnecessary because the final α is nearly $-\frac{1}{3}$. Furthermore, our published report involved two steps, the first being the assignment of W_0 *relative* to the maximum recoil momentum observed for each end point and the second being the adjustment of all constants to give a final *absolute* W_0. In the present work only the first step is critical. One can see that the important variable in the theoretical distribution is $Q^2/(W_0^2-1)=Q^2/Q^2(\max)$ where Q is the recoil momentum; thus, the critical uncertainty lies in the assignment of W_0 relative to the observed $Q(\max)$. If we denote the momentum calibration for a given preacceleration ratio by $\bar{Q}=K(2M_6V_d)^{1/2}=K'V_d^{1/2}$ then the pertinent uncertainty lies in W_0/K', and in the present analysis this ratio is chosen *independently* for the nonaccelerated and preaccelerated endpoints (*ibid.*, Fig. 2). The absolute value of W_0, $7.865m_0c^2$, enters in a secondary role.

The correction factor $R(x,\bar{E}_r)$ can now be estimated for energies below 1.3 keV by inserting the resolution functions from the end-point analyses into the integral of Eq. (7) and comparing the results with the linear

approximation. The resulting factor $R(x,\bar{E}_r)$ deviates significantly from unity only at recoil energies of 1.2 and 1.3 keV where the deviations are -0.1 and -0.5%, respectively, for preaccelerated ions and 0.0 and -0.2% for nonaccelerated ions. These resolution corrections would be valid even if the resolution function were skewed because the calibration refers to the center of gravity of the function.

D. Scattering in the Residual Gas

Arguments based on known cross sections were presented in Sec. 3 to show that the effects of scattering in the residual gas are negligible except in the magnet chamber. Experimental verification of this conclusion was obtained by a comparison of spectra observed under conditions of greatly increased pressure with values taken from a least-squares analysis of all measurements made at normal pressures; in both cases only nonaccelerated ions were used. Figure 7 shows the results in three sections, each of which pertains to a pressure increase in a separate element of the vacuum system. Figure 7(a) is consistent with the statement that the effects of scattering in the source are negligible; other similar measurements at high pressures support this conclusion. Figure 7(b) shows a loss for low-energy ions in the magnetic analyzer. The loss curve, which at 0.1 keV corresponds to an effective cross section of 20×10^{-16} cm^2/molecule, is drawn consistently with the data and with measurements by Cox[36] and by Thompson[37] on scattering of Li^+ ions in He and in Hg vapor. Above 0.6 keV, the curve is drawn with an E^{-1} dependence consistent with an r^{-2} scattering potential.[38] Figure 7(c) shows, as expected, a very small loss in the electrostatic analyzer. These curves, with the assumption of a linear pressure dependence, provide a correction factor $S(x\bar{E}_r)$ where $x\bar{E}_r$ is simply the energy of the ions in the analyzer.

E. Introduction of an Unknown Efficiency Parameter

All of the above corrections are small, and the central correction in the analysis is related to the detector's efficiency $M(x,y,\bar{E}_c)$. Ideally, the function would be measured independently with a precisely calibrated lithium ion source whose beam geometry duplicates that of the recoil ion beam; however, a precise calibration would be extremely difficult, requiring a very sensitive electrometer to give the source strength at a time when the detector is limited to about 10^4 ions/sec. No attempt was made to calibrate a source. Even in the absence of a precise calibration, no difficulty would arise if either y or $\bar{E}_c$ were absent from the efficiency function because one could then scan the recoil energy spectrum keeping

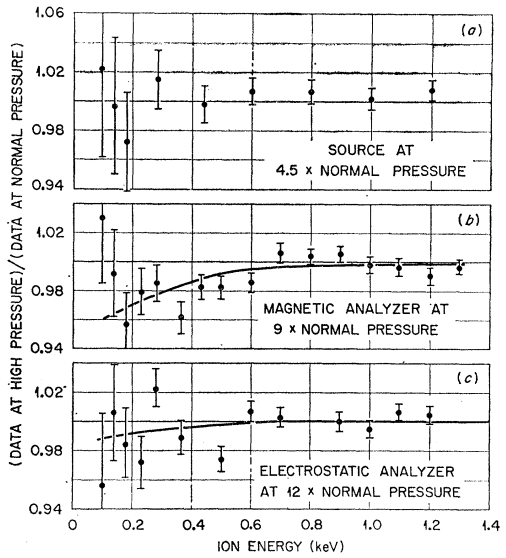

FIG. 7. Effects of elevated pressures in the source and analyzers for nonaccelerated ions. The data in the three graphs show the ratio of the counting rate at elevated pressures to the counting rate at normal pressures. In determining the ratios, the data for all measurements at normal pressures were replaced by a smooth least-squares fit. No significant scattering occurs in the source. Curves showing scattering effects in the analyzers are drawn partly on the basis of known scattering cross sections. Corrections based on these curves give 0.3% correction to α.

all variables except $\bar{E}_r$ constant. As will be shown, the detector efficiency has little y or $\bar{E}_c$ dependence; nevertheless, both are present and must be allowed for in the analysis.

A basic assumption is made that the detector variables y and $\bar{E}_c$ are separable,

$$M(x,y,\bar{E}_c)=B_3(x)G(y)C(\bar{E}_c). \tag{12}$$

This states, firstly, that the dependence on y and $\bar{E}_c$ is independent of the preacceleration ratio x. In other words, the same efficiency curves can be used for both non- and preaccelerated ions. This should be an excellent approximation because the width of the beam that is incident at the detector is always somewhat broader than the dimensions of the detector aperture; and, as shown in Sec. 3, this ion beam is only slightly narrowed by preacceleration. Probably $B_3(x)$ is constant, but this is not necessary. Secondly, the equation states that the transmission $G(y)$ of the grid structure for a given beam is only a function of the energy ratio $y=\bar{E}_c/\bar{E}_a$; there is no assumption here. Thirdly, and most important, the equation states that the probability of detection at the cathode is a function $C(\bar{E}_c)$ which is independent of the incident beam geometry, except for a possible multiplicative factor. This assumption should be valid. It is not very restrictive because it allows various parts of the cathode to differ in absolute efficiency, even to having zero efficiency, and demands only that the shape of the efficiency curve, which results by averaging over the beam, be independent of beam geometry. Actually the

[36] I. W. Cox, Phys. Rev. **34**, 1426 (1929).
[37] J. S. Thompson, Phys. Rev. **35**, 1196 (1930).
[38] J. H. Simons, C. M. Fontana, E. E. Muschlitz, Jr., and S. R. Jackson, J. Chem. Phys. **11**, 307 (1943).

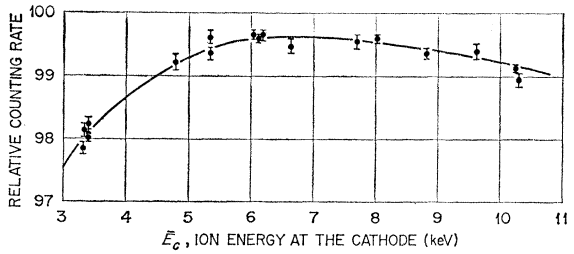

FIG. 8. Counting rate versus the ion energy at the cathode for a fixed energy ($\bar{E}_a$=2.6 keV) of the analyzed ions incident at the detector aperture. Data were obtained as ratios or average slopes; for each ratio two grid voltages were chosen and the counting rates were observed alternately and repeatedly at the two voltages. The ratios or slopes were then plotted to give a smooth curve and the uncertainties of counting statistics are given for the ratios. The curve is a function of both $\bar{E}_c$ and the energy multiplication $y=\bar{E}_c/\bar{E}_a$. Similar curves were obtained for several analyzer settings.

conditions for the assumption seem to be more than satisfied because the cathode surface appeared uniform and, as will be shown, the average efficiency varies only slightly with energy. The consistency of the data with this assumption is discussed later.

As shown in Appendix B, separation of variables leads to an unknown parameter μ_0 which is related to the slope of the cathode efficiency curve at some energy, say, $(\bar{E}_c)_0$. If the functions $G_\mu(x)$ and $C_\mu(\bar{E}_c)$ are derived from the data on the basis of an arbitrarily assumed constant, say $\mu=\mu_0+\delta$, then Eq. (10) becomes

$$B_4(x)\bar{E}_r^{(1-\delta)}N(\bar{E}_r,W_0,\alpha)=\frac{U'(\bar{E}_r,x,y)}{G_\mu(y)C_\mu(\bar{E}_c)}. \quad (13)$$

Here $U'(\bar{E}_r,x,y)$ is an abbreviation for the observed detector counts per monitor counts corrected for all effects other than the variation of detector efficiency. Although the detector parameter δ is unknown, it does appear in Eq. (13) in a well-defined form which follows from the separation of variable; thus, it can be included, along with the correlation coefficient and the normalization constant, as one of the adjustable parameters in the least-squares analysis. This, then, is our procedure: to determine the efficiency curves from extensive measurements, but for an arbitrary μ, and then to use Eq. (13) for a least-squares analysis with three adjustable parameters $B_4(x)$, δ, and α.

F. Measurements on the Detector Efficiency

Extensive measurements were made of the counting rates versus grid voltage at several fixed analyzer voltages. Data were obtained as ratios or average slopes; for each ratio two grid voltages were chosen and the counting rates were observed alternately and repeatedly at the two voltages. The uncertainties resulting from counting statistics are less than $\pm 0.2\%$ for some measurements and are believed to be a reliable measure of the random fluctuations.

Since the grid voltage was limited to 7.7 kV the curve of $G_\mu(y)$ was constructed by piecing together several overlapping segments obtained at various analyzer settings. For example, the first and most carefully measured segment for the 2-grid multiplier was obtained by preaccelerating 1.3-keV recoil ions to 2.6 keV for analysis and then observing the counting rates for grid voltages between 0.7 and 7.7 kV. Figure 8 shows the relative counting rate versus cathode energy for this example. The smooth curve is a visual fit to average slopes between various pairs of energies, and the indicated uncertainties from counting statistics refer to ratios. Values of $\bar{E}_c$ vary from 3.3 to 10.3 keV, but the y values vary only from 1.27 to 3.96. Thus, these measurements had to be followed by others at successively lower analyzer settings in order to extend the grid curve, step by step, to $y=37$.

An arbitrary average slope must then be chosen in order to plot $G_\mu(y)$ and $C_\mu(\bar{E}_c)$. We have chosen a slope such that $C_\mu(\bar{E}_c)$ rises 3% as $\bar{E}_c$ increases from 3.3 to 6.0 keV, and this single assumption allows us to plot the two curves, Figs. 9 and 10(a), for the 2-grid multiplier. The curve for the cathode efficiency $C_\mu(\bar{E}_c)$ results primarily from combining the assumed slope with the careful measurements in Fig. 8; and, given $C_\mu(\bar{E}_c)$, the observed ratios can then be used for a step-by-step plot of the grid function $G_\mu(y)$, beginning at $y=1.27$. Each statistical uncertainty in Fig. 10 refers to the ratio of a data point to some point on the smooth curve at lower y. Figure 10(b) shows the 3-grid function $G_\mu(y)$ which was obtained for the same arbitrary cathode slope. The cathode function $C_\mu(\bar{E}_c)$ was found to be the same as for the 2-grid counter, which was expected because precautions were taken to minimize the effects of cathode deterioration while the grid was being modified.

The dashed curves in Figs. 9 and 10 result from the least-squares estimate of δ which is obtained in the next section. It is seen that the 3-grid geometry almost satisfies the criterion that the grid function be independent of y.

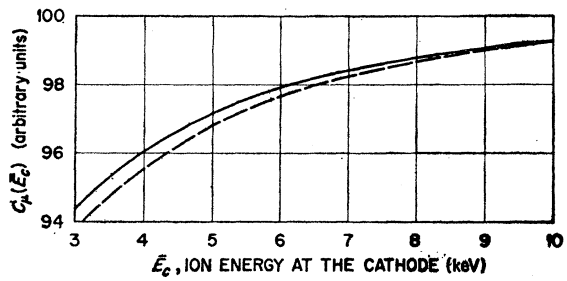

FIG. 9. Relative efficiency for detecting ions incident on the cathode. The solid curve was obtained from Fig. 8, and from other similar data, by choosing an average slope corresponding to a 3% rise between 3.3 and 6.0 keV. This slope enters into the analysis in a well-defined function and is one of the parameters subject to least-squares adjustment. The least-squares analysis gives the dashed curve.

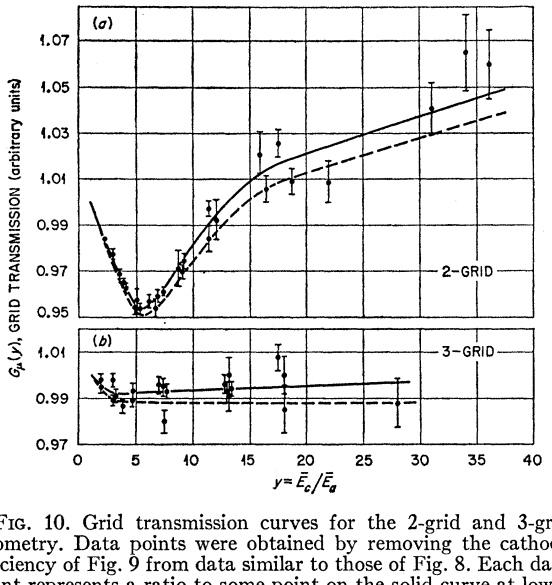

FIG. 10. Grid transmission curves for the 2-grid and 3-grid geometry. Data points were obtained by removing the cathode efficiency of Fig. 9 from data similar to those of Fig. 8. Each data point represents a ratio to some point on the solid curve at lower y value, and uncertainties are given by counting statistics. The solid curve and the data have been plotted in a stepwise manner beginning at the left. If the dashed curve in Fig. 9 had been used, the points would follow the dashed curve in the above figure.

G. The Composite Spectrum and the Least-Squares Analysis

As stated in Sec. 3 B, results of 26 observations of the spectra have been grouped according to the 12 modes of operation summarized in Table I. A detailed description of the modes of detector operation, other than that shown in the Table, will not be given. Essentially, they correspond to the use of various areas on the 3-dimensional efficiency surface, $G_\mu(y)C_\mu(\bar{E}_c)$. If the separation of variables is valid, then the results obtained in various parts of the surface will be consistent.

A composite spectrum is to be formed from the 12 sets of data with uncertainties based on the fluctuations among the 12 sets. Normalization factors for this purpose are found by making 12 least-squares three-parameter fits with the analytic expression in Eq. (13) and then integrating under the resulting curves. Such an integration weights each part of a spectrum approximately according to the counting statistics of the data points. Two comments are appropriate: First of all, the normalization factors vary from set to set for legitimate reasons which are associated with the degree of pre-acceleration, the grid structure, the length of the source, and a long-term drift of about 1% in monitor efficiency; and, secondly, the factors have little uncertainty, but this is not essential. If they were known exactly, the group of data points at each recoil energy in the composite spectrum would show the proper relative deviations, but if they are not known exactly, the points will deviate improperly, generally more than they should. In any case, improper normalization factors simply result in an apparent increase in the final random errors.

Small energy corrections are required for the composite spectrum. Data were customarily obtained at 16 particular frequencies for the magnetic resonance probe; but, as a result of the nonuniform hysteresis in the magnet, the corresponding 16 deflector voltages shifted slightly among the various sets. The energy derivatives required to shift all data to the final 16 energies were taken from a least-squares fit to all normalized points. The corrections have negligible uncertainties.

Thus, the original 12 sets of data, corrected for all of the effects that have been discussed, were normalized to form a single spectrum of 183 points at 16 energies. These points and their standard errors of counting statistics are now denoted $U_{kl}\pm\sigma_{kl}$ where k refers to the recoil energy $\bar{E}_k$, $k=1, 2, \cdots 16$, and l refers to a point at energy $\bar{E}_k$, $l=1, 2, \cdots n_k$. Values for n_k were listed in Table I. (For set 9, $n_k=27$.)

If the counting statistics were the only source of random fluctuations, this composite spectrum could be analyzed at once by the method of least-squares, weighting each point in proportion to σ_{kl}^{-2}. We know from our experience with the equipment, however, that the counting statistics alone do not account for all random effects; furthermore, one can easily show that the 183 points scatter about their 16 means more than is expected on the basis of counting statistics. For this reason we have bypassed the individual analyses of the 12 sets, except for the purpose of normalization, and gone directly to a composite spectrum whose uncertainties are derived from the actual fluctuations.

Appropriate weights w_{kl} are to be chosen in order to reduce the 183 datum points to 16 weighted means with associated standard errors, $U_k\pm\sigma_k$. Specifically,

$$U_k=\frac{\sum_l w_{kl}U_{kl}}{\sum_l w_{kl}}$$

and

$$\sigma_k^2=\frac{\sum_l w_{kl}(U_k-U_{kl})^2}{(n_k-1)\sum_l w_{kl}}. \tag{14}$$

In these equations, the weights σ_{kl}^{-2} would still be satisfactory if the counting statistics had not differed appreciably among the sets. In order to retain an appreciable contribution from all sets, weights are taken proportional to $\frac{1}{2}\sigma_{kl}^{-2}$ for data with preaccelerated ions and to σ_{kl}^{-2} for the nonaccelerated ions. The factor of $\frac{1}{2}$ has the effect of reducing the weights of the sets for preaccelerated ions from 85% of the total to about 70% of the total. In addition, the weights of 6 particular points for preaccelerated ions are reduced by an additional factor of 2 to 4. These 6 points, which were obtained with unusually good statistics, would otherwise dominate the groups of which they are members. The resulting σ_k's range from about 0.1% for the higher energy points to 0.7% for the lowest energy.

It is emphasized that these weights are not critical for estimating α. If the counting statistics had been used

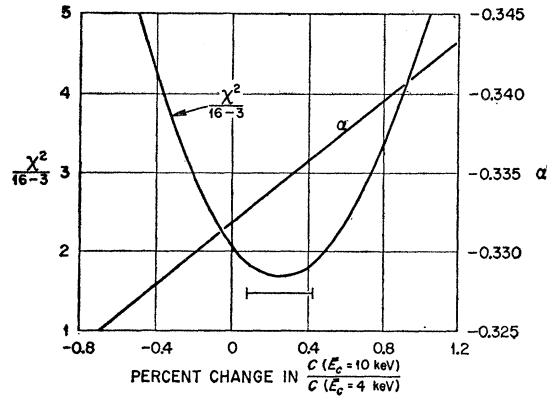

FIG. 11. Curves showing the effect of adjustment of the detector parameter. The abscissa is proportional to the detector parameter with zero corresponding to the solid curve in Fig. 9 and deviations from zero corresponding to a family of curves similar to the dashed line in Fig. 9. Least-squares adjustments of the normalization and correlation parameters for several values of the abscissa gave the parabola for $\chi^2/(16-3)$ and the straight line for values of α. The minimum for the parabola corresponds to $\alpha=-0.3343$, and the horizontal bar indicates the uncertainty for the least-squares fit.

directly in the least-squares analysis, the estimate of α would differ about 0.4% from that given here. The weights represent our best judgment for the estimation of α, but more importantly, they give a standard error and allow a χ^2 test on the basis of actual fluctuations.

The first three columns of Table III give the composite spectrum which is now analyzed by the method of least squares. The expected means from Eq. (13) are

$$\hat{U}_k=B\bar{E}_k{}^{(1-\delta)}N(\bar{E}_k,W_0,\alpha). \tag{15}$$

The parameters B, δ, and α are adjusted in order to minimize

$$Q^2=\sum_k(\hat{U}_k-U_k)^2/\sigma_k{}^2, \tag{16}$$

where the minimum is denoted χ^2. The least-squares analysis, using a nonlinear code,[39] gives an estimated correlation coefficient

$$\alpha=-0.3343\pm0.0017,$$

where the quoted uncertainty is found from the variance

$$\sigma^2=C^{-1}\chi^2/(16-3),$$

with C^{-1} representing the inverse diagonal matrix element for the parameter α.

Figure 11 demonstrates how the adjustment of the detector parameter δ has helped to achieve the minimum. The abscissa is proportional to δ, and the zero value corresponds to an analysis using the solid curves in Figs. 9 and 10. A deviation from zero means that $C_\mu(\bar{E}_c)$ would be altered from the solid curve by the indicated percentages. A correlated change would occur in the grid curves $G_\mu(y)$. The parabola showing χ^2 values was plotted from a series of 15 linear least-squares analyses of composite spectra based on 15 fixed values of δ and two adjustable parameters, B and $B\alpha$. The values of α derived from these fits fall on the straight line. As seen in the figure, the minimum for the curve agrees with the results of the nonlinear code. The horizontal error bar indicates the uncertainty in α given above.

The minimum for the 3-parameter analysis corresponds to the dashed curves in Figs. 9 and 10. Note that, if this estimate of the detector parameter had been guessed in the first place, the solid curve would have coincided with the dashed curves, and the data points would have followed the new solid curves. If these new curves had been used in correcting the data, the composite spectrum would have been given by the last column of Table III. It is of interest that if the dashed curves had been known to be correct, *a priori*, the uncertainty in α would be only ±0.0008; introduction of the adjustable detector parameter has doubled the estimated error.

TABLE III. The composite spectrum of data points $U_k\pm\sigma_k$ at the 16 recoil energies $\bar{E}_k$ has been derived on the basis of an arbitrary detector constant μ. These data were analyzed by the method of least squares in order to estimate the correct constant μ_0 as well as the correlation coefficient α. The right-hand column gives the data corrected according to the estimated μ_0, with arbitrary normalization. The analysis was actually made in terms of the recoil momentum Q with $W_0=7.865m_0c^2$ and $\bar{E}_k=23.303Q^2$ (energy in eV, momentum in m_0c units.)

$\bar{E}_k$ (eV)	U_k	σ_k	Corrected U_k
99.4	848.2	5.7	854.1
139.6	1372.7	8.4	1381.1
182.4	2026.9	9.0	2037.8
230.7	2809.6	3.3	2822.8
285.0	3734.8	15.0	3750.3
366.2	5214.5	9.8	5232.5
433.5	6453.5	9.8	6472.9
496.6	7625	12.5	7644
596.2	9384	8.8	9404
696.0	11 098	4.9	11 116
795.5	12 601	16.0	12 618
895.0	13 871	13.8	13 886
994.5	14 888	15.2	14 899
1093.2	15 605	17.7	15 613
1187.8	15 919	13.8	15 923
1293.0	15 381	20.0	15 381

H. Comments on Consistency

The least-squares analysis is based on the assumption that the observed spectrum results from random deviations from Eq. (15), and the estimated uncertainty reflects the random nature of the sample. Additional random and systematic uncertainties are discussed in the next section, but further unknown effects in the theory or experiment could invalidate Eq. (15). We can never say that the equation is "right," even though it has a very good physical basis, but we can ask questions regarding the consistency of the observations with the equation.

[39] B. W. Wood, ORGDP-K 1440, 1960 (unpublished).

Let us first make one check on the assumption of randomness in the least-squares procedure. Too few points were observed to give a meaningful check at each energy; however, the complete group of 183 points can be examined. The normal distribution at each energy should have an approximate width $\sigma_k n_k^{1/2}$, so that the frequency distribution of all of the ratios $(U_k - U_{kl})/(\sigma_k n_k^{1/2})$ should approximate a normal distribution of unit width. Indeed, it does.

Secondly, is the value of χ^2 from the analysis a reasonable result of random effects? The value of $\chi^2/(16-3)$ is 1.72, and a comparison with a χ^2 distribution shows that there is only a 5% probability that a random sample would give a value this large. This is a legitimate result of randomness; nevertheless, we should look for a clear reason for a large χ^2. Figure 12 shows the deviations of the data from the least-squares curve with the vertical height of each symbol representing σ_k. It happens that over half of the contribution to χ^2 comes from the two adjacent points with opposite deviations near 0.6 and 0.7 keV. Clearly any function chosen to reduce χ^2 would have an anomalous step near 0.65 keV; hence, we can reasonably conclude that the deviations are random or that the errors on these two points have been underestimated. In any case, since the estimated uncertainty in α includes the conventional factor $\chi^2/13$, the effects of these unusual fluctuations are included in the estimated error.

Finally, let us examine the measurements to see if the assumption of separation of detector variables should be suspected. This assumption, whose physical basis is given in Sec. 4 E, is important because it is the basis for introducing the third parameter δ into the analysis. Let us examine the efficiency curves. The fact that the least-squares analysis leads to a 3-grid focus curve that is essentially independent of y is significant; the observed counting rate curves all had nearly the same shape so that, *a priori*, little y dependence was expected. We can also ask if the efficiency curves are consistent with the data within the counting statistics. Let us treat the solid curves in Figs. 9 and 10 as if they were least-squares fits and estimate the degrees of freedom in order to make approximate χ^2 tests. The 3-grid curve for $G_\mu(y)$ could be represented by two intersecting straight lines having a total of three parameters (the normalization

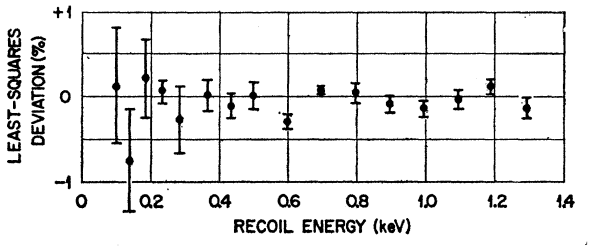

FIG. 12. The percentage deviations from the three-parameter least-squares fit to the composite spectrum. Uncertainties are based on the observed fluctuations among the 12 sets of data that were combined to give the spectrum.

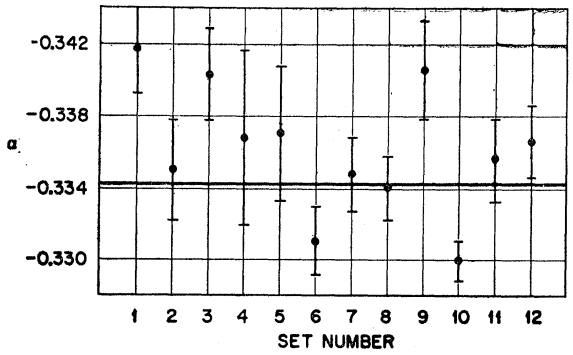

FIG. 13. Values of α from least-squares analyses of the 12 sets of data. In these analyses the detector parameter was fixed according to the dashed curves in Figs. 9 and 10. Uncertainties indicated by the heights of the symbols are assigned in a standard manner, and the horizontal line is the weighted mean of the 12 values. Fluctuations from the mean are greater than expected on the basis of these errors and indicate, primarily, a difference in end-point calibrations for the data with nonaccelerated and with preaccelerated ions. The error assignment in α for the composite spectrum includes the effect of these fluctuations.

at 100% is not one of these). The curve has 21 data points so that it has about 18 degrees of freedom. The more complicated 2-grid curve with 26 points has about 5 parameters or about 21 degrees of freedom. In this manner, we find $\chi^2/f \approx 1.14$ for the 2-grid curve and $\chi^2/f \approx 1.29$ for the 3-grid curves. Both are consistent with the expectation of about 1.0 ± 0.3 for a χ^2 distribution and, thus, are consistent with the assumption of separation of variables.

Another test of the separation of variables, as well as of other effects, is found by intercomparing the original 12 sets of data. If the separation of variables is valid, the detector has a constant μ_0 which is characteristic of the cathode. In order to intercompare the 12 sets we will choose the least-squares estimate of μ_0 corresponding to the dashed efficiency curves in Figs. 9 and 10. The least-squares analyses can then be made by adjustment of the remaining two parameters. Figure 13 shows the resulting 12 values of α with uncertainties given by $(\chi^2/f)C^{-1}$ where C^{-1} is the inverse diagonal matrix element for the parameter α. The weighted mean based on these errors is indicated by the solid line in the figure. Deviations from the mean are greater than would be expected on the basis of random fluctuations but do not indicate a failure of the assumption of separation of variables. For example, sets 1 through 5, which were obtained with nonaccelerated ions for various modes of detector operation, show good internal consistency. Sets 1 and 5 are particularly encouraging because they were obtained at a low value of $\bar{E}_c$, 2.2 keV, with the 2- and 3-grid counters, respectively. If there were cathode nonuniformities that might invalidate the assumption of separation of variables, their effect would be particularly offensive at the low energy of these two sets.

There is a systematic discrepancy between the data obtained with preacceleration and that obtained with-

TABLE IV. Uncertainties in the correlation coefficient.

Source of uncertainty	Uncertainty (%)
Random variations in the spectra	±0.5
Counting statistics of efficiency curves	±0.3
End-point uncertainties	±0.4
Resolution correction	±0.1
Voltage divider ratio	±0.1
Gas scattering correction	±0.15
Charge spectrum correction	±0.1
Anomalous monitor effect	±0.2
Stray magnetic fields	±0.2
Fierz term	±0.35
Standard error	±0.9

out, and this probably results from a difference in the independent end-point analyses for the two groups. The discrepancy was also apparent in the composite spectrum and is the reason for the large uncertainty in the highest energy point.

In summary of this section, the data generally show good internal consistency so that there is no reason to doubt the basic least-squares analysis. The twelve sets of data do show deviations outside of counting statistics, and this fact is reflected in the error assignment of the composite spectrum.

I. The Uncertainty in α

The final uncertainty of $\pm 0.9\%$ in α is estimated by combining several uncertainties, both random and systematic. Each systematic uncertainty is estimated in regard to some phase of the experiment, and the corresponding uncertainty in α is found by analyzing data which has been corrected according to the error limits. All errors are then combined in quadrature because they are each small and of unknown sign. Table IV summarizes the uncertainties in the order in which they are discussed below.

Random variations in the spectra, $\pm 0.5\%$. This uncertainty from the least-squares analysis includes not only random effects of counting statistics and other accidental fluctuations within each set of data but might also include unknown effects which are systematic in one set but vary randomly among the 12 sets.

Random variations in the efficiency curves, $\pm 0.3\%$. The efficiency curves were constructed from ratios whose uncertainties are given reliably by the counting statistics. The error which propagates to α was studied by a simple but tedious method in which the measurements were "repeated" by drawing numbers at random from normal distributions whose means are given by the solid efficiency curves in Fig. 10(a) or 10(b) and whose widths are equal to the standard error of counting statistics. New efficiency curves constructed from these "observed" ratios were then used in the analysis. This procedure, if repeated many times, would give an uncertainty in α resulting not only from the counting statistics but also from the variation in personal bias in drawing the curves. The method was repeated only three times for the 2-grid detector and four times for the 3-grid detector; but, since the resulting deviations are relatively small, these limited "observations" have been used to estimate the error.

End-point uncertainties, $\pm 0.4\%$. The critical end-point parameter W_0/K' (see Sec. 4 C) has a $\pm 0.04\%$ uncertainty for the data obtained without preacceleration ($x=1$), and, independently, $\pm 0.04\%$ for the data with preacceleration ($x\approx 2$). This statement may appear too optimistic for an analyzer whose momentum resolution width is 1.5% for nonaccelerated ions, and 2.2% for accelerated ions; nevertheless, the facts seem to demand this estimate. The evidence is, first of all, that a misfit caused by $\pm 0.04\%$ variation in W_0/K' is easily detected in the fitting of a particular set of data. Secondly, the data showed good reproducibility: Three measurements of the end point for nonaccelerated ions obtained over a two-month period gave a maximum deviation of 0.032% in W_0/K', and the two measurements with accelerated ions, which were obtained several weeks apart with different grid structures, differed by 0.01%. These results are based on curve fitting with given resolution functions; a further random uncertainty of $\pm 0.02\%$ is allowed for variations in the function. The $\pm 0.04\%$ uncertainty is an estimated standard error based on these results. The uncertainty for the composite spectrum is $\pm 0.033\%$ because it weights the independent measurements for non- and preaccelerated ions in the ratio of 1 to 2. A $\pm 0.34\%$ uncertainty is propagated to α. In addition, the absolute uncertainty in W_0 propagates a $\pm 0.06\%$ uncertainty to α. A total uncertainty of $\pm 0.4\%$ is assigned. Our confidence in this estimate is reinforced by an analysis which fixed α at $-\frac{1}{3}$ but allowed W_0 to be an adjustable parameter for a given analyzer calibration. This analysis, which ignores the end-point data, estimates W_0 to be 0.04% less than our accepted value and, thus, is consistent with our estimated error.

Finite energy resolution $\pm 0.1\%$. A small correction for finite energy resolution was required for the points near 1.2 and 1.3 keV. The error in these corrections has been estimated by the use of other possible resolution functions.

Voltage divider ratio, $\pm 0.1\%$. The analyzer calibration for most of the data was based on the same voltage divider that was used for the end-point measurement; however, the calibration at a few low energies was based on a different divider. The uncertainty in the intercomparison of these dividers propagates the above uncertainty to α.

Gas scattering correction, $\pm 0.15\%$. A complete analysis of the data without scattering corrections gives an estimated α of -0.3353; hence, the correction for scattering was 0.3%. The assigned uncertainty is one-half of the correction.

Charge spectrum correction, $\pm 0.1\%$. This is derived

from the experimental uncertainty given in Sec. 4 B for the energy dependence of the charge spectrum.

Anomalous monitor effect, ±0.2%. This corresponds to the limiting explanations to the monitor effect which was described in Sec. 3.

Stray magnetic field in the source volume, ±0.2%. The source should have been shielded against stray magnetic fields. Measurements with a Hall probe after the experiment was terminated showed that the field was nearly zero at both ends of the source but rose to 0.3 G at the center. Calculations show that this field causes negligible error if the various baffles in the spectrometer are properly aligned. If the baffles are unaligned, the percentage change in transmission, either loss or gain, is inversely proportional to the momentum of the ion. We have assumed, pessimistically, that the most important baffle in the magnet chamber could have been off by ±0.4 in. so that the counting rates could be in error by about ±1% for 0.1-keV recoil ions and less for higher energy ions. This assumption leads to the ±0.2% error in α. Our confidence in this estimate is increased as the result of an analysis which included an adjustable, magnetic-field parameter. The theoretical spectrum was multiplied by $(1+\gamma E_k^{-1/2})$ with γ being adjustable. The resulting α agreed to 0.3% with the 3-parameter analysis, and χ^2 was reduced very little by the presence of the fourth parameter. Finally, measurements[24] with Na^{23} recoil ions whose momentum was equivalent to 250-eV Li^6 ions showed a (0.5±0.8)% difference in transmission for measurements with and without magnetic shielding on the source. These results are all consistent with there being no error resulting from the stray magnetic field.

Fierz term, ±0.35%. The foregoing analysis was made under the assumption that the Fierz term β is zero. Ramaswamy[30] found from a reinvestigation of the decay of Na^{22} that $\beta=-0.004\pm0.012$ for Gamow-Teller transitions. For reasons of simplicity, we have assigned the uncertainty on the basis of the symmetric limits, $\beta=0.0\pm0.012$.

The uncertainty in the correction for dead time losses is negligible, about ±0.01%.

5. CONCLUSION

The results of these measurements give the correlation coefficient

$$\alpha=-0.3343\pm0.0030,$$

where the uncertainty is our best estimate of the standard error. With the assumption that the polarization of the β^- particles is $-v/c$, the polarization of the antineutrino becomes

$$P_{\bar{\nu}}=(100.3\pm0.9)\%.$$

These results are certainly consistent with the presently accepted $V-A$ theory.

An interpretation to give a limit to the tensor interaction is made by use of Bayes' theorem of inverse probability,[40] which can be written

$$P_\alpha(\alpha_0)=P(\alpha_0)P_{\alpha_0}(\alpha), \tag{17}$$

where

$$\int_{-\infty}^{+\infty} P_\alpha(\alpha_0)d\alpha_0=1.$$

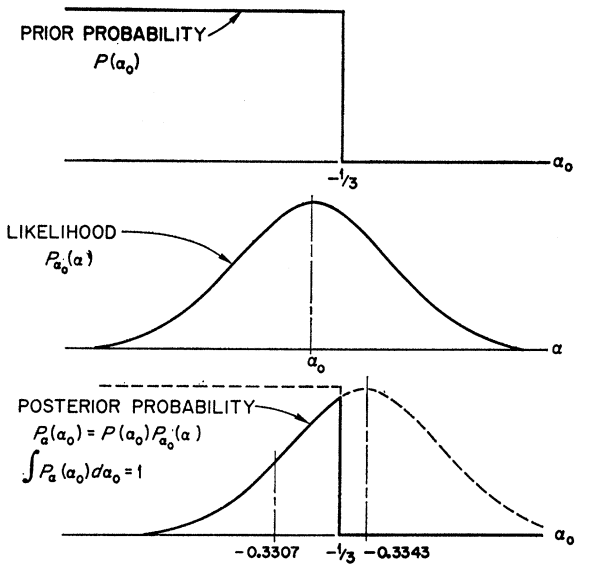

FIG. 14. A graphic representation of the prior probability, likelihood, and posterior probability which form the basis for the conclusion on the limit of tensor interaction. The reader may have other prior knowledge or concepts and thus may choose a different prior probability from that suggested here.

These equations state that, given a measured α, the posterior probability $P_\alpha(\alpha_0)$ for the true value being α_0 is equal to the product of the prior probability $P(\alpha_0)$ multiplied by the likelihood $P_{\alpha_0}(\alpha)$ for observing a value α. The normalization integral states that there is an α_0. We assume that only random effects cause α to differ from the true α_0; hence, the likelihood function can be represented as a normal distribution.

The prior probability should be a mathematical statement of all prior knowledge. This statement is not easily formulated, but a fair approximation is made by assuming that the coefficient must be within the Gamow-Teller limits. As reviewed in the Introduction, other experimental measurements that determine the relative strengths of the tensor and axial-vector coupling constants do not have precision approaching the present measurement so that their omission will not seriously alter our conclusion. Thus, our prior knowledge is that, for an allowed Gamow-Teller transition with negligible second-forbidden interference terms, α_0 lies between $+\frac{1}{3}$ and $-\frac{1}{3}$. There may be various ways to state this prior knowledge; we state

$$\begin{aligned} P(\alpha_0)d\alpha_0 &\propto d\alpha_0 \quad \text{for} \quad |\alpha_0|\leqslant\tfrac{1}{3} \\ &=0 \quad \text{for} \quad |\alpha_0|>\tfrac{1}{3}. \end{aligned}$$

[40] Sir Harold Jeffreys, *Theory of Probability* (Clarendon Press, Oxford, England, 1961), 3rd ed., Chap. I.

The resulting posterior probability distribution, which is illustrated in Fig. 14, is the tail of a normal distribution of width $\sigma=0.0030$ centered at $\alpha_0=-0.3343$. Only that part of the distribution which lies within the G.T. limits is allowed and its area is normalized to unity. The most probable value of α_0 is -0.3333, and the limits $-0.3307\geqslant\alpha_0\geqslant-0.3333$ contains 68% of the posterior probability distribution. The corresponding limit for the tensor interaction, from Eq. (5), is

$$\frac{|C_T|^2+|C_T'|^2}{|C_A|^2+|C_A'|^2}\leqslant 0.4\%.$$

Further remarks on this subject are given in Appendix C.

No experiment has shown that the tensor interaction is absent; nevertheless, abundant experimental and theoretical information suggest very strongly that it is. We now assume $C_T=C_T'=0$ (a new prior probability) in order to discuss second order effects which appear in the conserved vector current theory. Gell-Mann,[25] on the basis of the fact that the vector current is conserved, introduced a weak magnetism term a which has been experimentally verified.[41–43] Terms in a do not appear in the recoil energy spectrum[44]; however, a parameter b from Gell-Mann's paper on weak magnetism does appear. Huffaker and Greuling[45] have treated b further in a theory related to the axial-vector part of the weak interaction. If there are no induced nuclear structure form factors, b is equal to $1/2M$ where M is the ratio of the nucleon to electron mass; however, Huffaker and Greuling have found from a theoretical analysis of the data on μ capture in C^{12} and the ratio of $B^{12}-N^{12}ft$ values that Gell-Mann's b is about $-4.4/2M$. A correct theory of the electron-neutrino correlation is not available for $Z\neq 0$; however, Gell-Mann gives expressions for the plane-wave ($Z=0$) approximation. A theoretical recoil energy spectrum with $\alpha=-\frac{1}{3}$ and with an unknown parameter b is easily obtained from his expressions; and, to a very good approximation, can be considered simply by replacing α in our equations by α', where

$$\alpha'=-\frac{1}{3}\left(1-\frac{8W_0b}{3}\right). \tag{18}$$

Thus, we conclude, assuming the prior probability that b can have any value,

$$b=-(0.5\pm 1.3)(2M)^{-1}.$$

(The error assignment now includes no Fierz term uncertainty because $\beta=0$ in this theory.) This value is about one-tenth of Huffaker and Greuling's estimate. A more complete theory including other small effects might alter our conclusion.

ACKNOWLEDGMENTS

We are indebted to Dr. A. H. Snell and Dr. J. L. Fowler for their continued interests and discussions and to Dr. T. A. Welton, Dr. R. L. Becker, and Dr. E. Greuling for their help in the interpretation of the measurements. We are particularly grateful to Dr. Greuling for his guidance in the treatment of small theoretical effects. We are indebted to many members of the ORNL Mathematics Panel for their extensive help in the least-squares analyses. Barry Preedom contributed appreciably to an understanding of the experimental equipment and R. L. Hamner provided the BeO powder and allowed us to use his laboratory in the preparation of the He^6 generator.

APPENDIX A

Explicit formulas for the functions in the theoretical recoil energy distribution, Eq. (4), are given here. Although the recoil energy E_r is the variable used throughout this report, the recoil momentum Q is more convenient and more fundamental in the theory. In terms of Q the functions are, with $X\equiv W_0^2-Q^2$,

$$N_1(Q)dQ=N_1(E_r)dE_r=Q^2\frac{(X-1)^2}{(X)^3}\times[X(X-1)+2W_0^2(X+2)]dQ, \tag{A1}$$

$$N_2(Q)dQ=N_2(E_r)dE_r=\left[N_1(Q)-6Q^2\frac{(X-1)^2}{X}\right]dQ, \tag{A2}$$

and

$$N_3(Q)dQ=N_3(E_r)dE_r=[6Q^2W_0(X-1)^2/X^2]dQ. \tag{A3}$$

APPENDIX B

The assumption of separation of the detector variables was introduced in Sec. 4 E and a new parameter was introduced into the analysis. The proof of the recoil energy dependence for that parameter is given here. For simplicity the average energies $\bar{E}_r$ and $\bar{E}_c$ are written E_r and E_c. As in Eq. (14), let $U'(E_r,x,y)$ denote the counting rates corrected for all minor effects and consider the limit in which the rate is a continuous function of its variables. From Eqs. (10) and (13)

$$E_rN(E_r,W_0,\alpha)=\frac{U'(E_r,x,y)}{B(x)G(y)C(E_c)}, \tag{B1}$$

where

$$E_c=xyE_r.$$

[41] T. Mayer-Kuckuk and F. C. Michel, Phys. Rev. **127**, 545 (1962).
[42] Y. K. Lee, L. W. Mo, and C. W. Wu, Phys. Rev. Letters **10**, 253 (1963).
[43] N. W. Glass and R. W. Peterson, Phys. Rev. **130**, 299 (1963).
[44] Eugene Greuling and M. E. Rose first showed us that a vanishes in the recoil spectrum.
[45] J. N. Huffaker and Eugene Greuling, Phys. Rev. **132**, 738 (1963).

Take the logarithms and differentiate with respect to E_r:

$$\frac{d[\ln E_r N(E_r,W_0,\alpha)]}{dE_r}dE_r$$
$$=\frac{\partial[\ln U'(E_r,x,y)]}{\partial E_r}dE_r-E_c\frac{d\ln C(E_c)}{dE_c}\frac{dE_r}{E_r}. \quad \text{(B2)}$$

Integration from $E_r=E_0$, $x=x_0$ to E_r, x_0 along the line $(E_c)_0=x_0yE_r$ yields

$$E_rN(E_r,W_0,\alpha)=C_0E_r^{-\mu_0}g(E_r), \quad \text{(B3)}$$

where

$$C_0=E_0^{(1+\mu_0)}N(E_0,W_0,\alpha),$$
$$\mu_0=(E_c)_0\frac{d\ln C(E_c)}{dE_c}\bigg|_{(E_c)_0},$$

and

$$g(E_r)=\exp\left[\int_{E_0}^{E_r}\frac{\partial[\ln U'(E_r,x,y)]}{\partial E_r}\bigg|_{x_0,(E_c)_0}dE_r\right].$$

The function $g(E_r)$ is, in principle, the observable of our experiment. Of course, we did not measure $g(E_r)$ in exactly the manner prescribed by the above integral; but, rather, we observed $U'(E_r,x,y)$ with limited statistics at many discrete points in the (E_r,x,y) space. Except for the limitations of counting statistics, the measurements overdetermine $g(E_r)$.

The constant μ_0 was not measured and could not be measured without a source with a known energy spectrum. If μ_0 were known and $G(y)$ and $G(E_c)$ were derived from the data on the basis of this known constant, then Eq. (B1) could be used. Since μ_0 is not known, our procedure is to derive efficiency curves $G_\mu(y)$ and $C_\mu(E_c)$ from the data on the basis of an arbitrary constant, say $\mu=\mu_0+\delta$. Then from Eq. (B1) and (B3),

$$E_r^{(1-\delta)}N(E_r,W_0,\alpha)=C_0E_r^{-(\mu_0+\delta)}g(E_r)$$
$$=C_1\frac{U'(E_r,x,y)}{B(x)G_\mu(y)C_\mu(E_c)}, \quad \text{(B4)}$$

where the proportionality constant depends on the normalization of the efficiency curves. The increment δ is an adjustable parameter in the least-squares analysis.

APPENDIX C

In regard to Bayes' theorem of inverse probability, it is appropriate to acknowledge the fact that statisticians are divided into two opposing schools of thought. Many statisticians reject Bayes' theorem as used by Jeffreys and take the frequency approach. They would consider our measurement as a random sample from an infinite parent group whose members are normally distributed in a curve of width $\sigma=0.0030$ about the unknown true value α_0. The infinite parent group is a mathematical abstraction; clearly a large number of experimentalists will not repeat these measurements and, even if they do, their average result will be only one measurement in a new, narrower parent group. Given our measurements, this school would describe the region between the error limits as a 68% *confidence interval* and consider the value -0.3343 to be the best estimate of α_0. Clearly, under the theory in which α was determined, α_0 cannot be -0.3343. At the same time the value of -0.3343 is a legitimate observation; if, for example, $\alpha_0=-\frac{1}{3}$, then repeated measurements should scatter on both sides of $-\frac{1}{3}$. Those who take the frequency approach can draw no conclusion regarding the limit of the tensor interaction.

We accept Bayes' theorem. In this approach one must accept the presence of prior knowledge and be willing to combine this knowledge with the new information in order to make plausible conclusions. This approach has been developed to a high level by Jeffreys[40] and others but it also embodies "common sense" which is closely related to prior probability.

A few additional remarks are pertinent. If there were no knowledge about α_0, then we would have assumed that the prior probability is a constant, $P(\alpha_0)d\alpha_0=kd\alpha_0$, and would have concluded within 68% *posterior probability* that α_0 is within the quoted error limits and that -0.3343 is the most probable value. On the surface, both schools reach the same conclusion in this case. We note also that the limit on the T interaction would have been even smaller on the basis of our assumed prior probability if α were even more negative. The reader might conclude that our procedure is ridiculous because, if α had been observed further from the "right answer," a smaller limit could have been given for the tensor interaction. The reader in this case simply does not believe our statement of prior knowledge or of likelihood but is injecting his own information or common sense into the conclusion. Rightly so! Our statement of prior probability is an approximation not including possible second-order theoretical effects and our statement of likelihood does not include possible systematic experimental errors. Certainly, if α were removed from the Gamow-Teller limit by several times the standard errors, we would look more closely for missing knowledge; however, since the observed α is nearly $-\frac{1}{3}$, the exact form of the prior probability or likelihood is not critical.